# Comparison of Two Optimization Techniques for the Estimation of Complex Permittivities of Multilayered Structures Using Waveguide Measurements

Michael E. Baginski, *Senior Member, IEEE*, Daniel L. Faircloth, *Student Member, IEEE*, and Manohar D. Deshpande, *Senior Member, IEEE*

***Abstract*—In this paper, two separate techniques, i.e., sequential quadratic programming (SQP) and a genetic algorithm (GA), were used to estimate the complex permittivity of each layer in a multilayer composite structure. The relative performance of the algorithms was characterized by applying each algorithm to one of three different error functions. Computer generated $S$-parameter data sets were initially used in order to establish the achievable accuracy of each algorithm. Based on these data sets and $S$-parameter measurements of single and multilayer samples obtained using a standard $X$-band waveguide procedure, the GA was determined to be the more robust algorithm in terms of minimizing rms error of measured/generated and formulated $S$-parameters. The GA was found to perform exceptionally well for all cases considered, whereas SQP, although a more computationally efficient method, was somewhat limited for two error function choices due to local minima trapping.**

***Index Terms*—Genetic algorithm (GA), multilayered substrate, permittivity extraction, sequential quadratic programming (SQP).**

## I. Introduction

MULTILAYER substrate materials are currently used for many practical applications that include microwave integrated circuits (MICs), monolithic microwave integrated circuits (MMICs) [1], radomes, spatial filters for antenna beam shaping [2], and frequency-selective surfaces (FSSs) [3].

By choosing the appropriate thicknesses and material parameters for the layers, it is possible to synthesize composite structures with novel electromagnetic properties otherwise not found in a single material [4]. Recently, attention has focused on nondestructive methods of determining the constitutive parameters of each individual layer of the substrate [5], [6].

There are a large number of methods for determining the permittivity or permeability of a single homogeneous sample or the effective "bulk" properties of a layered material. These methods include split-cylinder resonators, cavity resonators, $\mathrm{TE}_{10}$ split-post dielectric and magnetic resonators, whispering-gallery resonators, transmission-line and waveguide techniques, etc. [7]–[9]. For measurements of the complex permittivity and permeability over broad frequency bands (e.g., $X$- or $L$-bands), transmission line or waveguide methods are generally preferred even though the achievable accuracy is reduced due to unavoidable measurement errors [4], [10].

Some recent methods used to accurately estimate the complex permittivity of individual layers of a multilayered or inhomogeneous structure are given by Sanadiki and Mostafavi [11], Zwick *et al.* [6], and Deshpande and Dudley [4]. Sanadiki and Mostafavi provide a method of solving the inverse scattering problem using a least squares error approach. This method is only tested against computer-generated data and may be sensitive to errors associated with measurements. Zwick *et al.* utilize a genetic algorithm (GA) to find the complex constitutive parameters for a multilayered sample by an evolutionary process. Their method requires measurements be obtained over a frequency range or as a function of incidence angle for a given frequency and does not require phase information for the transmission or reflection coefficients. Deshpande and Dudley's algorithm employs sequential quadratic programming (SQP) and utilizes both magnitude and phase information of the measured $S$-parameters, which, in turn, requires very accurate system calibration.

In this paper, the performance of two optimization techniques, i.e., SQP and GA, are evaluated when applied to the multilayer complex permittivity extraction problem using $S$-parameter measurements obtained from a loaded waveguide. Additionally, their sensitivity and performance relative to the choice of error function is investigated. Simulations are performed using computer-generated $S$-parameters to quantify the performance of each algorithm under ideal conditions. In order to determine the robustness of these methods, the extracted permittivities determined by the algorithms are used to generate $S$-parameter data sets for comparison to the measured $S$-parameters.

$S$-parameter $X$-band waveguide measurements were made using the following dielectric materials: Bakelite, ceramic, Garlock rubber, and nanomaterial. All of the materials are low-loss, nonmagnetic, and were found to have complex permittivities that remained nearly constant over the $X$-band [4]. They were used to create planar single-layer samples of various thicknesses with all samples having $X$-band waveguide cross-sectional dimensions. The multilayer dielectric structures were fabricated by placing single-layer samples adjacent to one another (see Fig. 1). All measurements were obtained using an HP-8510C vector network analyzer for frequencies

Manuscript received April 12, 2005; revised June 22, 2005. This work was supported by the National Aeronautics and Space Administration (NASA) Langley Research Center.

M. E. Baginski and D. L. Faircloth are with the Department of Electrical and Computer Engineering, Auburn University, AL 36849 USA.

M. D. Deshpande is with the NASA Langley Research Center, Hampton, VA 23681 USA.

Digital Object Identifier 10.1109/TMTT.2005.855133

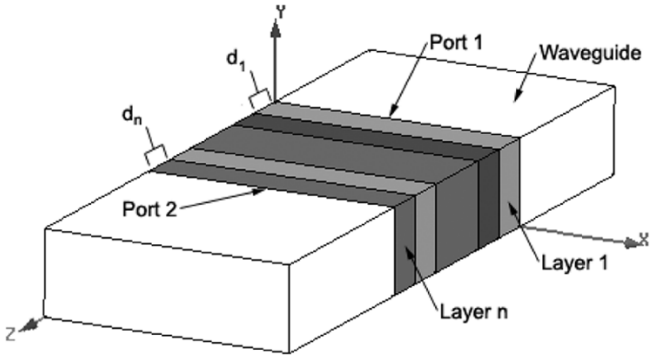


Fig. 1. Rectangular waveguide loaded with $n$-layer sample.

of 8.2–12.4 GHz ($X$-band). Additionally, the complex permittivity of each single-layer sample was determined using the Agilent 85071 Materials Measurement Software [12], [13] and compared to the values obtained from the algorithms.

## II. Fundamental Theory

Assuming that only the dominate $\mathrm{TE}_{10}$ mode propagates in the loaded waveguide (see Fig. 1), the formulation of the $S$-parameters can be expressed in terms of each layer's thickness $(d_n)$ and unknown permittivity $(\hat{\epsilon}_n)$ using $ABCD$-parameters as follows [14], [15]:

$$\begin{bmatrix} A_n & B_n \\ C_n & D_n \end{bmatrix} = \begin{bmatrix} \cosh(\gamma_n d_n) & Z_n \sinh(\gamma_n d_n) \\ \dfrac{\sinh(\gamma_n d_n)}{Z_n} & \cosh(\gamma_n d_n) \end{bmatrix} \quad (1)$$

$$\begin{bmatrix} A & B \\ C & D \end{bmatrix} = \prod_{i=1}^{n} \begin{bmatrix} A_i & B_i \\ C_i & D_i \end{bmatrix} \quad (2)$$

where $\gamma_n$ and $Z_n$ are the propagation constant and wave impedance of the $n$th layer, respectively, and given as

$$Z_n = \frac{j\omega\mu}{\gamma_n} \quad (3)$$

$$\gamma_n = \sqrt{\left(\frac{\pi}{a}\right)^2 - \omega^2 \mu \hat{\varepsilon}_c} \quad (4)$$

where $a$ is the appropriate (maximum) cross-sectional dimension of the waveguide.

The $ABCD$-parameters can be directly converted to $S$-parameters using the following equations:

$$S_{11} = \frac{\left(A + \dfrac{B}{Z_0} - CZ_0 - D\right)}{X}$$

$$S_{12} = \frac{2(AD - CB)}{X}$$

$$S_{21} = \frac{2}{X}$$

$$S_{22} = \frac{\left(-A + \dfrac{B}{Z_0} - CZ_0 + D\right)}{X}$$

$$X = A + \frac{B}{Z_0} + CZ_0 + D \quad (5)$$

where $Z_0$ is the empty waveguide impedance.

### A. Error-Function Selection

The error functions used in the investigation are of the following basic form:

$$\mathrm{Err} = \sqrt{\frac{1}{N}\sum_{i=1}^{N}\left[f([\mathbf{S}]_{f,i}) - f([\mathbf{S}]_{m,i})\right]^2} \quad (6)$$

where $N$ is the total number of frequency points, $[\mathbf{S}]_{f,i}$ are the formulated $S$-parameters (5) evaluated at frequency point $i$, and $[\mathbf{S}]_{m,i}$ are the measured $S$-parameters at frequency point $i$. Error functions can generally be grouped into two categories, which are: 1) error functions used to minimize differences in both phase and magnitude of the measured and formulated scattering parameters and 2) error functions that minimize only magnitude variations of the measured and formulated scattering parameters. It is beyond the scope of this research to contrast the performance of all possible variants of error function definitions used in previous research for permittivity extraction. For the purposes of this research, three error function definitions were used and found to accurately obtain the permittivity of single and multilayer structures shown in (7)–(9) at the bottom of this page, where

$$M_i = \left(|[S]_{f,i}| - |[S]_{m,i}|\right)^2$$

$$P_{f1,i} = 1 - |S_{11}|^2_{f,i} - |S_{21}|^2_{f,i}$$

$$P_{f2,i} = 1 - |S_{22}|^2_{f,i} - |S_{12}|^2_{f,i}$$

$$P_{m1,i} = 1 - |S_{11}|^2_{m,i} - |S_{21}|^2_{m,i}$$

$$P_{m2,i} = 1 - |S_{22}|^2_{m,i} - |S_{12}|^2_{m,i}$$

$$\mathrm{Err} = \sqrt{\frac{1}{N}\sum_{i=1}^{N}\left(\left(\mathrm{Re}\left([\mathbf{S}]_{f,i}\right) - \mathrm{Re}\left([\mathbf{S}]_{m,i}\right)\right)^2 + \left(\mathrm{Im}\left([\mathbf{S}]_{f,i}\right) - \mathrm{Im}\left([\mathbf{S}]_{m,i}\right)\right)^2\right)} \quad (7)$$

$$\mathrm{Err} = \sqrt{\frac{1}{N}\sum_{i=1}^{N}\left(\left|[\mathbf{S}]_{f,i}\right| - \left|[\mathbf{S}]_{m,i}\right|\right)^2} \quad (8)$$

$$\mathrm{Err} = \sqrt{\frac{1}{N}\sum_{i=1}^{N} M_i + P_{1,i} + P_{2,i}} \quad (9)$$

$$P_{1,i} = \left(P_{f1,i} - P_{m1,i}\right)^2$$
$$P_{2,i} = \left(P_{f2,i} - P_{m2,i}\right)^2.$$

Equation (7) includes both phase and magnitude information. It is a slightly modified form of Deshpande and Dudley's error function [4] and is applicable to materials where the permittivity remains approximately constant over the measured frequency range. The inclusion of measurement information over the entire frequency range minimizes the effects of instrumentation error in the calculations. Equation (8) requires only magnitude information of the scattering parameters and is representative of the fitness (error) function used by Zwick *et al.* [6] and Queffelec and Gelin [8]. The third error function (9) is unique in that it uses only magnitude information, but includes terms accounting for dissipated power. It was initially believed that the inclusion of the power terms would increase the algorithms' ability to accurately determine the imaginary part of the permittivity. It should be noted that (8) and (9) are calculated in decibels, which was found to decrease the time required to find the global minimum in the solution space [6].

### *B. Discussion of the Optimization Methods*

A significant amount of time was devoted to finding accurate, yet computationally efficient methods of minimizing the error functions (7)–(9). Some of the more robust optimization procedures considered were the Levenberg–Marquardt (LM) algorithm [16], SQP [17], simulated annealing [18], and GAs [19]. All of the algorithms were investigated for their ability to obtain the complex permittivity using computer generated $S$-parameter data for multilayer structures. SQP and the GA provided the most accurate solutions for their respective classes of optimization methods and were, therefore, chosen for the study.

*1) SQP:* SQP is relatively easy to implement and is considered to be one of the most robust nonlinear programming (NP) methods available for optimization problems [20]. Following every iteration, the Hessian and Lagrangian operators are approximated and used to create a quadratic programming subproblem. The solution of the subproblem is the basis for the formation of the line search direction. Depending on the accuracy of the initial guess, SQP can exhibit a rapid second-order convergence toward a local minimum. Unfortunately, SQP, being a local optimization method, can suffer from local minima trapping even when upper and lower bounds are specified [20]. SQP has been discussed in detail by [17], [21]–[24].

*2) GA:* The GA was originally based on the concept of natural selection and, therefore, much of the terminology is related to the field of evolutionary biology. GAs, like many other global optimization techniques (e.g., simulated annealing), overcome the problem of local minima trapping by introducing some element of randomness. For an in-depth discussion of GAs and their application to electrical engineering problems, the reader is referred to [19], [25], and [26]. The remainder of this section discusses the specific GA implemented in this research.

The GA begins by generating a population of permittivity values randomly distributed throughout the solution space (see Fig. 2). Each member of the population, referred to as a chromosome, contains a complex permittivity value for every layer of the multilayer problem being considered. Every permittivity

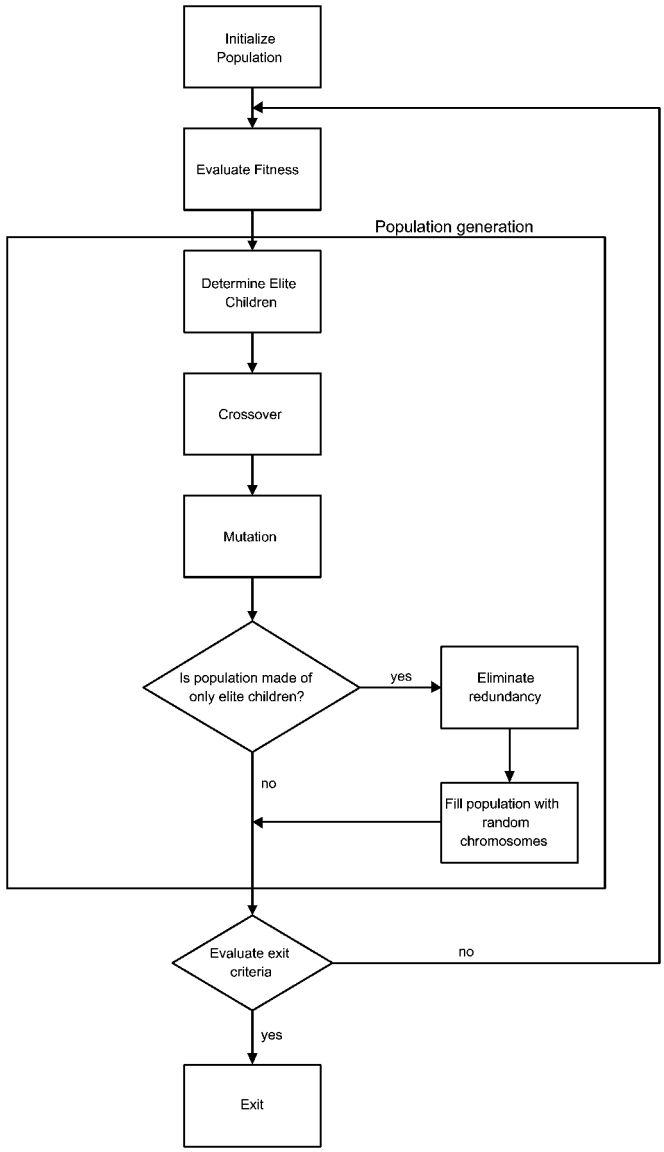


Fig. 2. Flowchart illustrating the GA procedure.

value (gene) stored in a chromosome is encoded as a 16–bit binary string, thereby allowing traditional crossover and mutation schemes to be implemented. Upon generation of the initial population, the fitness of each chromosome is determined by evaluating the error function. The fitness value of the chromosome is defined as the value of the error function.

After fitness evaluation, a new population (generation) is created. Construction of the new population begins by selecting a subset population representing the "best" chromosomes (i.e., those chromosomes having the lowest error function value). These "elite" chromosomes are inserted into the new population ensuring that these solutions will not be eliminated from the new generation.

The crossover stage is the defining phase of the GA. First, two "parent" chromosomes are selected from the current generation using the binary tournament selection method [26]. Following selection of the parent chromosomes, the GA generates a random number $p \in [0, 1]$. If $p > p_{\text{crossover}}$, the crossover rate, the two parents are copied directly into the new population.

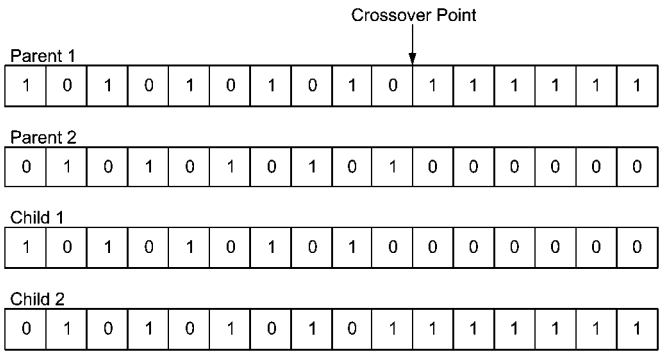


Fig. 3. Crossover using binary string encoding.

Otherwise, a random position in the parents' binary string of encoded information is selected (see Fig. 3). The first "child" is formed using the string of information to the left of the crossover point in the first parent and the information to the right of the crossover point in the second parent. The second child is formed using the remaining genetic information from each parent. This process of selection and crossover is repeated until the new population is completed. Using this concept, chromosomes with poor fitness that possibly possess "good" genetic information have the opportunity to pass their traits on to future generations.

The next major phase of the GA is the mutation stage. For each child in the new population (elite children excluded), a random number $m \in [0, 1]$ is generated. If $m > p_{\text{mutation}}$, the mutation rate, no change is made to the chromosome. However, if $m < p_{\text{mutation}}$, one or two random bits of the chromosome are transposed (i.e., $1 \leftrightarrow 0$). This reduces the likelihood of local minima trapping.

After a significant number of generations, the GA converges to a population consisting of identical chromosomes representing the best obtained solution to the fitness function (with the exception of the occasional mutation). At this point, a traditional GA exits since simple mutation alone is a very inefficient way of searching for new genetic information that will more effectively minimize the error function. In this research, however, the GA checks for this redundancy in the population for each new generation. When this situation occurs, one duplicate copy of this redundant chromosome is kept as well as any mutations. The rest of the population slots are filled with random chromosomes in the same manner in which the initial population was generated and the algorithm is restarted. This technique was found to enhance the GA's ability to find the global minimum.

The GA will discontinue if a chromosome is found to have a fitness value below $10^{-5}$ or if the maximum number of generations has been reached. Depending on the number of layers being characterized, the maximum number of generations is allowed to vary. The specific details of this parameter's selection will be discussed in Section IV.

## III. Measurement Setup

$X$-band measurements of the $S$-parameters for the loaded rectangular waveguide (cross-sectional dimensions 22.86 × 10.16 mm) were made using the experimental setup shown in Fig. 4. Errors due to the instrumental setup (coaxial adapters, losses, etc.) are minimized using the standard calibration procedure suggested for the HP-8510C vector network analyzer [27], [28]. Calibration requires a series of standards for the procedure that allow the effects of all connectors and losses to be identified. Once this is completed, the measurements are taken without the need for further data processing. A brief description of the calibration procedure is given as a courtesy to the reader in the Appendix.

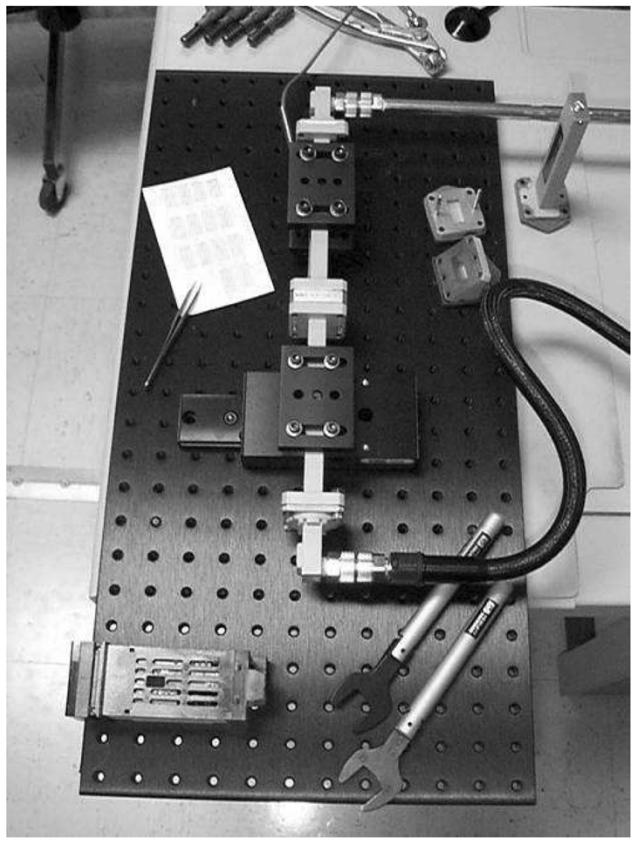

Fig. 4. Waveguide measurement setup.

TABLE I
Complex Permittivities and Thicknesses for the One-, Two-, and Three-Layer Computer-Generated Data Sets

| Layer | $\hat{\varepsilon}_n$ | $d_n$ (mm) |
|---|---|---|
| 1 | $7 - j0.01$ | 1 |
| 2 | $3 - j0.02$ | 10 |
| 3 | $2 - j0.1$ | 2 |

## IV. Results

### A. Computer-Generated $S$-Parameters

Computer-generated $S$-parameter data sets for one-, two-, and three-layer cases over $X$-band frequencies were initially used to test the accuracy of each extraction scheme. The respective complex permittivities and thicknesses are shown in Table I (single-layer permittivity extraction used layer 1; two-layer extraction used layers 1 and 2; three-layer extraction used all layers ordered accordingly). The initial complex permittivity guess for all layers was set to $\hat{\varepsilon}_{\text{initial}} = 5 - j0.4$, while the search space for both algorithms was limited to $1 < \text{Re}\,(\hat{\varepsilon}_c) < 10$ and $0 < \text{Im}\,(\hat{\varepsilon}_c) < 0.8$.

TABLE II
RESULTS USING IDEAL $S$-PARAMETERS

| Algorithm | Objective | Error Function | One Layer | | Two Layers | | Three Layers | |
|---|---|---|---|---|---|---|---|---|
| | | | Error | Time (s) | Error | Time (s) | Error | Time (s) |
| SQP | Single | ( 7) | 1.837e-9 | 59.1 | 1.729e-8 | 4.3 | 2.431e-8 | 6.8 |
| | | ( 8) | 2.702e-8 | 1.9 | 1.780e-7 | 65.6 | X | X |
| | | ( 9) | 1.959e-11 | 50.1 | 1.396e-7 | 65.6 | X | X |
| | Multiple | ( 7) | 1.712e-13 | 2.1 | 2.012e-9 | 72.7 | 6.245e-9 | 83.3 |
| | | ( 8) | 6.397e-9 | 54.4 | 8.538e-8 | 4.4 | X | X |
| | | ( 9) | 2.183e-9 | 54.2 | 1.656e-7 | 3.1 | X | X |
| GA | Single | ( 7) | 3.561e-7 | 68.8 | 2.636e-4 | 969 | 2.079e-4 | 6467.2 |
| | | ( 8) | 3.106e-6 | 103.1 | 2.003e-3 | 1136.4 | 1.151e-2 | 9683.3 |
| | | ( 9) | 3.147e-6 | 124.7 | 7.266e-3 | 2059 | 1.058e-2 | 11715 |

The SQP algorithm terminated for error function or directional derivative values $\leq 10^{-16}$ or after 5000 iterations. The GA's population size was set to a value of 100 and terminated after 200, 1000, and 5000 generations for the one-, two-, and three-layer cases, respectively. The GA utilized an 80% crossover rate and 10% mutation rate (these values are within the range of nominal values given by [26]).

In Table II, the results for the one-, two-, and three-layer cases using each algorithm (single or multiobjective) and error function are shown. An "X" in the table indicates that the algorithm extracted incorrect complex permittivity values for the indicated sample (i.e., the algorithm became trapped in a local minimum). For the multiobjective cases, each term in the error functions (7)–(9) becomes an element of an error function vector. For instance, in a multiobjective format, (8) would then be given by

$$\overrightarrow{\mathrm{Err}} = \begin{bmatrix} \sqrt{\frac{1}{N}\sum_{i=1}^{N}\left(|S_{11,f,i}| - |S_{11,m,i}|\right)^2} \\ \sqrt{\frac{1}{N}\sum_{i=1}^{N}\left(|S_{21,f,i}| - |S_{21,m,i}|\right)^2} \\ \sqrt{\frac{1}{N}\sum_{i=1}^{N}\left(|S_{12,f,i}| - |S_{12,m,i}|\right)^2} \\ \sqrt{\frac{1}{N}\sum_{i=1}^{N}\left(|S_{22,f,i}| - |S_{22,m,i}|\right)^2} \end{bmatrix}. \quad (10)$$

The vectorization of the error functions was expected to increase the sensitivity of the SQP algorithm.

The results shown in Table I indicate that all methods performed extremely well for the single- and double-layer complex permittivity extraction. However, permittivity extraction for the three-layer sample was unsuccessful using SQP with error functions (8) and (9). This is due to local minimum trapping indicating a poor initial estimate (guess) of the complex permittivity. Alternatively, the GA was able to successfully extract complex permittivity values using all three error functions independent of the number of layers. It should also be noted that the error for both the real and imaginary parts of the complex permittivity is less than $O(10^{-7})$ for the SQP using (7) and less than $O(10^{-3})$ for the GA using any of (7)–(9) for the one-, two-, and three-layer cases.

### B. Single-Layer Measurements

For measurements of single-layer materials, samples of Bakelite ($d = 3.277$ mm), ceramic ($d = 2.845$ mm), Garlock rubber ($d = 1.702$ mm), and nanomaterial ($d = 3.099$ mm) were used. $S$-parameter data sets were generated using the extracted permittivity value from each algorithm and then compared to the measured $S$-parameter values. Additionally, the Agilent 85071 Materials Measurement Software was used to extract the single-layer permittivities for comparison to the values returned by the SQP and GA algorithms.

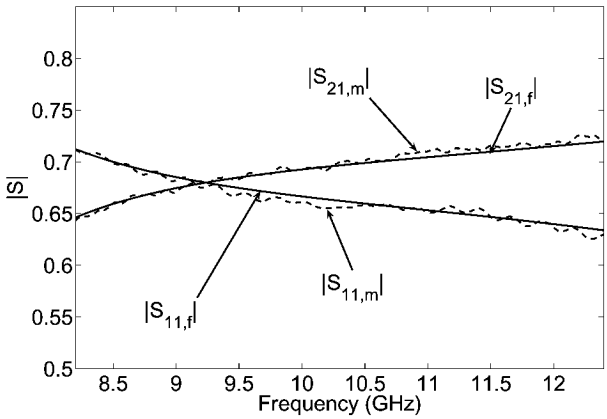


Fig. 5. Magnitude of $S_{11}$ and $S_{21}$ for single-layer Bakelite sample. The calculated $S$-parameters are generated using the GA with error function (9).

Fig. 5 shows a comparison of $|S_{11}|$ and $|S_{21}|$ for the measured $S$-parameters of the Bakelite sample and those generated from the extracted permittivities returned by the GA using error function (9). Fig. 6 shows similar results for the Garlock sample. The excellent agreement shown in Figs. 5 and 6 is also observed for all other materials' $S$-parameter comparisons using all algorithm/error function combinations.

Tables III–VI show the results of the extracted complex permittivities for each material using all optimization algorithms and error functions. Since error functions (8) and (9) are calculated in decibels, a direct comparison of the error function values is not necessarily indicative of the accuracy of the solution. Rather, summations of the rms errors between the magnitudes and phases of the formulated and measured $S$-parameters (see columns 6 and 7 in Tables III–VI) are better qualifiers of the accuracy of each solution as follows:

$$\sum_{ij}\sqrt{|S_{ij,f}|^2 - |S_{ij,m}|^2}$$
$$\sum_{ij}\sqrt{\left(\angle S_{ij,f}\right)^2 - \left(\angle S_{ij,m}\right)^2}. \quad (11)$$

The rms errors between the measured $S$-parameters and those generated using the Agilent 85071 Materials Measurement Soft-

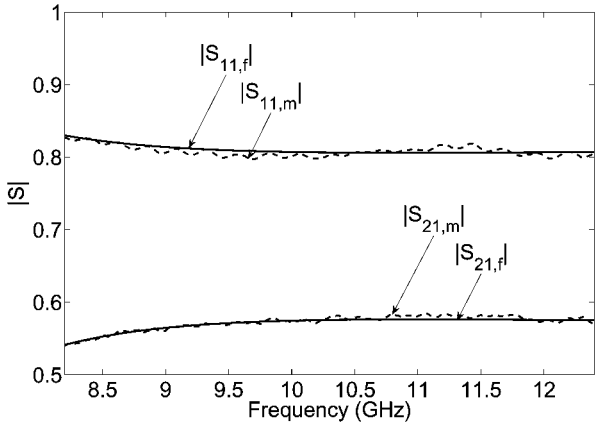


Fig. 6. Magnitude of $S_{11}$ and $S_{21}$ for single-layer Garlock rubber sample. The calculated $S$-parameters are generated using the GA with error function (9).

TABLE III
EXTRACTED PERMITTIVITY AND ERROR FOR BAKELITE

| Algorithm | Objective | Error Function | $\varepsilon'$ | $\varepsilon''$ | $\sum \lvert S_{ij}\rvert_{err}$ | $\sum \angle S_{ij_{err}}$ |
|---|---|---|---|---|---|---|
| SQP | Single | ( 7) | 3.7244 | 0.2237 | 0.02875 | 0.19899 |
| | | ( 8) | 3.7907 | 0.2528 | 0.01339 | 0.20948 |
| | | ( 9) | 3.7909 | 0.2530 | 0.01339 | 0.20952 |
| | Multiple | ( 7) | 3.5124 | 0.3464 | 0.09824 | 0.29814 |
| | | ( 8) | 3.7896 | 0.2656 | 0.01434 | 0.20685 |
| | | ( 9) | 3.8018 | 0.2577 | 0.01364 | 0.21206 |
| GA | Single | ( 7) | 3.7244 | 0.2238 | 0.02876 | 0.19898 |
| | | ( 8) | 3.7907 | 0.2528 | 0.01339 | 0.20948 |
| | | ( 9) | 3.7910 | 0.2530 | 0.01339 | 0.20954 |
| 85071 | X | X | 3.6032 | 0.2347 | 0.06947 | 0.24004 |

TABLE IV
EXTRACTED PERMITTIVITY AND ERROR FOR CERAMIC

| Algorithm | Objective | Error Function | $\varepsilon'$ | $\varepsilon''$ | $\sum \lvert S_{ij}\rvert_{err}$ | $\sum \angle S_{ij_{err}}$ |
|---|---|---|---|---|---|---|
| SQP | Single | ( 7) | 1.1422 | 0.0000 | 0.03263 | 0.15330 |
| | | ( 8) | 1.1819 | 0.0004 | 0.00415 | 0.19111 |
| | | ( 9) | 1.1819 | 0.0006 | 0.00415 | 0.19151 |
| | Multiple | ( 7) | 1.1344 | 0.0000 | 0.03888 | 0.14662 |
| | | ( 8) | 1.1782 | 0.0518 | 0.04234 | 0.70040 |
| | | ( 9) | 1.1823 | 0.0050 | 0.00670 | 0.21894 |
| GA | Single | ( 7) | 1.1423 | 0.0000 | 0.03261 | 0.15333 |
| | | ( 8) | 1.1818 | 0.0001 | 0.00417 | 0.18989 |
| | | ( 9) | 1.1820 | 0.0010 | 0.00422 | 0.19331 |
| 85071 | X | X | 1.1484 | 0.0043 | 0.02802 | 0.18255 |

ware are also listed for comparison. It can be concluded that all of the optimization techniques were effective in minimizing the rms errors of the $S$-parameters (both phase and magnitude). However, the GA using either (8) or (9) was found to consistently produce the lowest magnitude error of the $S$-parameters (column VI) and maintained a phase error no worse than the other extraction methods.

### C. Two-Layer Measurements

The two-layer structures used for the $S$-parameter measurements were Garlock rubber/Bakelite, Garlock rubber/ceramic, and Garlock rubber/nanomaterial with Garlock rubber used as the first layer for all cases. As discussed in Section IV-B, the three error functions (7)–(9) were minimized using SQP and the GA. No change was made to any parameter of the SQP

TABLE V
EXTRACTED PERMITTIVITY AND ERROR FOR GARLOCK RUBBER

| Algorithm | Objective | Error Function | $\varepsilon'$ | $\varepsilon''$ | $\sum \lvert S_{ij}\rvert_{err}$ | $\sum \angle S_{ij_{err}}$ |
|---|---|---|---|---|---|---|
| SQP | Single | ( 7) | 7.7850 | 0.0409 | 0.04200 | 0.13297 |
| | | ( 8) | 7.9837 | 0.1642 | 0.01669 | 0.17187 |
| | | ( 9) | 8.1358 | 0.1304 | 0.02075 | 0.20980 |
| | Multiple | ( 7) | 7.6184 | 0.0869 | 0.06706 | 0.08846 |
| | | ( 8) | 8.0340 | 0.1604 | 0.01425 | 0.18396 |
| | | ( 9) | 8.0347 | 0.1602 | 0.01424 | 0.18415 |
| GA | Single | ( 7) | 7.6184 | 0.0869 | 0.06707 | 0.08846 |
| | | ( 8) | 8.0340 | 0.1604 | 0.01425 | 0.18396 |
| | | ( 9) | 8.0348 | 0.1602 | 0.01424 | 0.18417 |
| 85071 | X | X | 7.5320 | 0.1610 | 0.08267 | 0.06454 |

TABLE VI
EXTRACTED PERMITTIVITY AND ERROR FOR NANOMATERIAL

| Algorithm | Objective | Error Function | $\varepsilon'$ | $\varepsilon''$ | $\sum \lvert S_{ij}\rvert_{err}$ | $\sum \angle S_{ij_{err}}$ |
|---|---|---|---|---|---|---|
| SQP | Single | ( 7) | 2.5165 | 0.0000 | 0.05783 | 0.08785 |
| | | ( 8) | 2.5989 | 0.0119 | 0.01058 | 0.18065 |
| | | ( 9) | 2.5989 | 0.0119 | 0.01058 | 0.18061 |
| | Multiple | ( 7) | 2.4916 | 0.0000 | 0.07457 | 0.06210 |
| | | ( 8) | 2.5842 | 0.0000 | 0.01671 | 0.15915 |
| | | ( 9) | 2.5837 | 0.0064 | 0.01530 | 0.16201 |
| GA | Single | ( 7) | 2.5165 | 0.0000 | 0.05779 | 0.08791 |
| | | ( 8) | 2.5989 | 0.0119 | 0.01057 | 0.18069 |
| | | ( 9) | 2.5989 | 0.0119 | 0.01057 | 0.18069 |
| 85071 | X | X | 2.6872 | 0.0260 | 0.05989 | 0.27670 |

algorithm, whereas the GA was allowed 1000 generations before termination. The extracted permittivities were used to generate $S$-parameters data sets for rms error computation and were also contrasted to the Agilent 85071 results of Section IV-B. It should be mentioned that the Agilent 85071 software can only determine the permittivity of single materials or provide bulk permittivity estimates for composite structures.

Tables VII–IX show the extracted permittivities and $S$-parameter rms errors for the three two-layer samples. Using two-layer $S$-parameter data sets generated from the single-layer Agilent 85071 extracted permittivities, the rms error between these data sets and the measured $S$-parameters was calculated and is also included in these tables. For the Garlock rubber/Bakelite sample, all algorithm/error function combinations achieved rms magnitude errors $O(10^{-2})$ and phase errors $O(10^{-2}$–$10^{-1})$. The magnitude of the extracted permittivities for each layer showed excellent agreement with the extracted single-layer values. However, the imaginary part of the extracted permittivity for Garlock rubber showed an increased value when compared to the values given in Table V.

For the Garlock rubber/ceramic and Garlock rubber/nanomaterial samples (see Tables VIII and IX), the SQP algorithm was only effective at estimating the complex permittivity values using error function (7). Using error functions (8) and (9), SQP was unable to correctly estimate each layer's complex permittivity despite achieving a low magnitude rms error. It is apparent from the discrepancies in the estimated permittivity values and the large $S$-parameter phase errors that this was a result of local minimum trapping. Unlike SQP, the GA was successful in extracting the complex permittivities using all error functions. The real and imaginary parts of the permittivities showed excellent agreement with the extracted single-layer values, and the

TABLE VII
EXTRACTED PERMITTIVITY AND ERROR FOR GARLOCK/BAKELITE

| Algorithm | Objective | Error Function | Garlock $\varepsilon'$ | Garlock $\varepsilon''$ | Layer 2 $\varepsilon'$ | Layer 2 $\varepsilon''$ | $\sum \lvert S_{ij}\rvert_{err}$ | $\sum \angle S_{ij_{err}}$ |
|---|---|---|---|---|---|---|---|---|
| SQP | Single | ( 7) | 7.9050 | 0.2207 | 4.0271 | 0.3274 | 0.0400 | 0.0647 |
| | | ( 8) | 7.5613 | 0.3626 | 3.9900 | 0.2563 | 0.0366 | 0.1997 |
| | | ( 9) | 7.8488 | 0.3343 | 3.9881 | 0.2583 | 0.0387 | 0.1036 |
| | Multiple | ( 7) | 7.8211 | 0.3080 | 4.0086 | 0.2908 | 0.0379 | 0.0991 |
| | | ( 8) | 7.9793 | 0.2813 | 3.9827 | 0.2980 | 0.0410 | 0.0699 |
| | | ( 9) | 7.9793 | 0.2813 | 3.9827 | 0.2980 | 0.0410 | 0.0699 |
| GA | Single | ( 7) | 7.9050 | 0.2207 | 4.0271 | 0.3274 | 0.0400 | 0.0647 |
| | | ( 8) | 7.5620 | 0.3625 | 3.9900 | 0.2563 | 0.0366 | 0.1994 |
| | | ( 9) | 7.8523 | 0.3336 | 3.9883 | 0.2585 | 0.0387 | 0.1027 |
| 85071 | X | X | 7.5320 | 0.1610 | 3.6032 | 0.2347 | 0.1136 | 0.3289 |

TABLE VIII
EXTRACTED PERMITTIVITY AND ERROR FOR GARLOCK/CERAMIC

| Algorithm | Objective | Error Function | Garlock $\varepsilon'$ | Garlock $\varepsilon''$ | Layer 2 $\varepsilon'$ | Layer 2 $\varepsilon''$ | $\sum \lvert S_{ij}\rvert_{err}$ | $\sum \angle S_{ij_{err}}$ |
|---|---|---|---|---|---|---|---|---|
| SQP | Single | ( 7) | 7.9478 | 0.1169 | 1.2254 | 0.0373 | 0.0268 | 0.0601 |
| | | ( 8) | 1.0000 | 0.0712 | 6.1163 | 0.0963 | 0.0687 | 6.3055 |
| | | ( 9) | 1.0000 | 0.1167 | 6.1037 | 0.0656 | 0.0695 | 6.3189 |
| | Multiple | ( 7) | 7.8983 | 0.0405 | 1.2596 | 0.0649 | 0.0378 | 0.0686 |
| | | ( 8) | 1.0000 | 0.2616 | 6.1208 | 0.0066 | 0.0732 | 6.3536 |
| | | ( 9) | 1.0000 | 0.2616 | 6.1208 | 0.0066 | 0.0732 | 6.3536 |
| GA | Single | ( 7) | 7.9479 | 0.1169 | 1.2254 | 0.0373 | 0.0268 | 0.0601 |
| | | ( 8) | 8.0688 | 0.1916 | 1.1930 | 0.0000 | 0.0144 | 0.0639 |
| | | ( 9) | 8.0866 | 0.1927 | 1.2167 | 0.0000 | 0.0146 | 0.0654 |
| 85071 | X | X | 7.5320 | 0.1610 | 1.1484 | 0.0043 | 0.0803 | 0.1267 |

TABLE IX
EXTRACTED PERMITTIVITY AND ERROR FOR GARLOCK/NANOMATERIAL

| Algorithm | Objective | Error Function | Garlock $\varepsilon'$ | Garlock $\varepsilon''$ | Layer 2 $\varepsilon'$ | Layer 2 $\varepsilon''$ | $\sum \lvert S_{ij}\rvert_{err}$ | $\sum \angle S_{ij_{err}}$ |
|---|---|---|---|---|---|---|---|---|
| SQP | Single | ( 7) | 7.6909 | 0.1382 | 2.7840 | 0.0585 | 0.0307 | 0.0490 |
| | | ( 8) | 2.5193 | 0.1860 | 5.4421 | 0.0110 | 0.0178 | 6.5273 |
| | | ( 9) | 2.5193 | 0.1978 | 5.4555 | 0.0020 | 0.0178 | 6.5223 |
| | Multiple | ( 7) | 7.6700 | 0.1435 | 2.7751 | 0.0380 | 0.0308 | 0.0552 |
| | | ( 8) | 2.4387 | 0.1856 | 5.3484 | 0.0152 | 0.0217 | 6.5841 |
| | | ( 9) | 2.4729 | 0.1596 | 5.4659 | 0.0147 | 0.0204 | 6.5315 |
| GA | Single | ( 7) | 7.6909 | 0.1382 | 2.7841 | 0.0585 | 0.0307 | 0.0490 |
| | | ( 8) | 7.7636 | 0.2344 | 2.6881 | 0.0142 | 0.0132 | 0.0942 |
| | | ( 9) | 7.7544 | 0.2510 | 2.6866 | 0.0068 | 0.0136 | 0.0972 |
| 85071 | X | X | 7.5320 | 0.1610 | 2.6872 | 0.0260 | 0.0294 | 0.1103 |

TABLE X
EXTRACTED PERMITTIVITY AND ERROR FOR NANOMATERIAL/GARLOCK/GARLOCK

| Algorithm | Objective | Error Function | Layer 1 $\varepsilon'$ | Layer 1 $\varepsilon''$ | Layer 2 $\varepsilon'$ | Layer 2 $\varepsilon''$ | Layer 3 $\varepsilon'$ | Layer 3 $\varepsilon''$ | $\sum \lvert S_{ij}\rvert_{err}$ | $\sum \angle S_{ij_{err}}$ |
|---|---|---|---|---|---|---|---|---|---|---|
| SQP | Single | ( 7) | 2.8234 | 0.0615 | 8.3424 | 0.2413 | 8.1992 | 0.2086 | .03571 | .06789 |
| | | ( 8) | 2.9228 | 0.0064 | 8.2085 | 0.3069 | 7.3469 | 0.3813 | .01132 | .28668 |
| | | ( 9) | 2.9255 | 0.0133 | 8.1900 | 0.3014 | 7.3365 | 0.3561 | .01178 | .28771 |
| | Multiple | ( 7) | 2.7634 | 0.0371 | 8.3823 | 0.3812 | 8.3505 | 0.3224 | .05696 | .06735 |
| | | ( 8) | 4.1458 | 0.0082 | 4.7201 | 0.2681 | 2.2123 | 0.8000 | .23606 | 3.6167 |
| | | ( 9) | 4.6797 | 0.0000 | 2.4478 | 0.6366 | 2.8608 | 0.0000 | .14824 | 4.5302 |
| GA | Single | ( 7) | 2.8238 | 0.0625 | 8.3417 | 0.2402 | 8.1981 | 0.2051 | .03568 | .06775 |
| | | ( 8) | 2.9159 | 0.0125 | 8.1326 | 0.3000 | 7.4216 | 0.3630 | .01254 | .26070 |
| | | ( 9) | 2.9259 | 0.0136 | 8.1716 | 0.3000 | 7.3279 | 0.3552 | .01185 | .29188 |
| 85071 | X | X | 2.6872 | 0.0260 | 7.5320 | 0.1610 | 7.5320 | 0.1610 | .10697 | .63053 |

GA achieved rms magnitude errors $O(10^{-2})$ and phase errors $O(10^{-2}$–$10^{-1})$.

### *D. Three-Layer Measurements*

The $S$-parameters for a three-layer composite structure (nanomaterial/Garlock rubber/Garlock rubber) were measured. As was done previously, Table X shows the extracted permittivities and $S$-parameter rms errors for the composite structure. SQP was effective in determining the complex permittivities of the sample for all but the multiobjective form of (8) and (9). As in the previous sections, the GA successfully estimated the permittivities using all error functions. SQP and the GA returned rms magnitude errors $O(10^{-2})$ and phase errors $O(10^{-2}$–$10^{-1})$.

It was already determined that the algorithms and error functions would return complex permittivity values nearly indistinguishable from the actual values for all computer generated cases (SQP using (8) and (9) was excepted). Therefore, the possible reasons for the errors sited previously warrant an explanation. The authors believe that the most likely sources of error

for the single-layer extractions stem from inaccuracies associated with instrumentation and sample thickness measurements. In addition to these errors, compound structures may suffer from the presence of small air gaps between the layers, as well as sample misalignment. Also, results obtained using (7) will be adversely affected by any uncertainty in the phase planes' positions.

## V. Conclusions

In this paper, the performance of complex permittivity extraction methods based on SQP and the GA was contrasted using $S$-parameter measurements for one-, two-, and three-layer samples. Three different error function definitions were also used to quantify the performance of each algorithm in terms of the amount of $S$-parameter information (magnitude only or magnitude and phase) available for the inversion process.

Computer-generated $S$-parameter data was initially used to determine the attainable accuracy of each algorithm/error function combination. The results of this portion of the study clearly indicated that the extracted permittivity from the single-layer and multilayer cases was nearly identical to that used to generate the data when the GA was used. This was also found to be true for SQP in all but two cases due to local minima trapping. This demonstrates that the GA is extremely accurate and would, therefore, be limited only by the precision of the $S$-parameter measurements, whereas the performance of SQP would also likely be limited by the accuracy of the initial guess.

The algorithm/error functions were used to extract the complex permittivity from single-layer $S$-parameter measurements and it was evident that all of the optimization techniques were highly effective at minimizing the rms error(s) of the $S$-parameters (both phase and magnitude). However, the GA using either (8) or (9) was found to consistently produce the lowest magnitude error of the $S$-parameters, whereas (7) routinely yielded the lowest phase errors and only slightly larger magnitude errors. The likely reason for this result is that both magnitude and phase information are explicitly included in (7), and only magnitude information is included in (8) and (9). Therefore, if phase information is available from a given measurement setup, (7) would likely produce the most accurate material characterization. Nevertheless, if only measured $S$-parameter magnitude information is available, accurate results may still be obtained using (8) and (9).

When the same techniques were used for complex permittivity extraction from multilayer composite structures, the GA, for all cases considered, provided approximately the same level of accuracy as that observed for the single-layer cases. SQP, however, failed to obtain accurate results for several of the cases considered. In summary, the GA appeared to be the more robust algorithm in terms of its ability to always achieve a low $S$-parameter rms error and accurately obtain each layer's complex permittivity.

## Appendix
## RF Measurement Calibration

Instrumentation errors are determined as the difference between the measured and known responses of a set of standards. Using the suggested thru-reflect-line (TRL) approach [28], the impedance mismatch at the coaxial adapters can be determined and factored out of the measurements. The calibration plane is established in the loaded waveguide, preferably at the interface of the sample. Therefore, impedance discontinuities created by the test sample in the waveguide are determined directly. Determination of the calibration plane is required for each sample.

During the calibration procedure, a short circuit is connected at the end of the access waveguide at each port. For the calibration of input to port 1 and output at port 2, the network analyzer is connected with the two access waveguides. For the step "line," a short length of waveguide is inserted between the access waveguides. After the calibration process, the sample holder containing the test sample is inserted between the access waveguides, and the waveguides are aligned. This procedure is necessary to establish the precise location of the reference planes for $S$-parameter measurements and is repeated when the ports are reversed.

## References


[1] K. Gupta and P. S. Hall, *Analysis and Design of Integrated Circuit-Antenna Modules*. New York: Wiley, 1999.

[2] S. Chakravarty and R. Mittra, "Application of the micro-genetic algorithm to the design of spatial filters with frequency-selective surfaces embedded in dielectric media," *IEEE Trans. Electromagn. Compat.*, vol. 44, no. 2, pp. 338–346, May 2002.

[3] S. Chakravarthy, R. Mittra, and N. Williams, "Application of the micro-genetic algorithm to the design of spatial filters with frequency-selective surfaces embedded in dielectric media," *IEEE Trans. Antennas Propag.*, vol. 50, no. 3, pp. 284–296, Mar. 2002.

[4] M. D. Deshpande and K. Dudley, "Estimation of complex permittivity of composite multilayer material at microwave frequency using waveguide measurements," NASA Langley Res. Center, Hampton, VA, USA, NASA Tech. Memo. 212 398, 2003.

[5] C.-W. Chang, K.-M. Chen, and J. Qian, "Nondestructive determination of electromagnetic parameters of dielectric materials at $X$-band frequencies using a waveguide probe system," *IEEE Trans. Instrum. Meas.*, vol. 46, no. 10, pp. 1084–1092, Oct. 1997.

[6] T. Zwick, J. Haala, and W. Wiesbeck, "A genetic algorithm for the evaluation of material parameters of compound multilayered structures," *IEEE Trans. Microw. Theory Tech.*, vol. 50, no. 4, pp. 1180–1187, Apr. 2002.

[7] M. D. Janezic and J. Baker-Jarvis, "Full-wave analysis of a split-cylinder resonator for nondestructive permittivity measurements," *IEEE Trans. Microw. Theory Tech.*, vol. 47, no. 10, pp. 2014–2020, Oct. 1999.

[8] P. Queffelec and P. Gelin, "New method for determining the permeability tensor of magnetized ferrites in a wide frequency range," *IEEE Trans. Instrum. Meas.*, vol. 48, no. 8, pp. 519–522, Aug. 2000.

[9] C. J. Reddy, M. D. Deshpande, and G. A. Hanidu, "Learning tool for estimation of complex permittivity of dielectric material," in *Proc. Frontiers in Education Conf.*, Nov. 1996, pp. 1195–1196.

[10] M. D. Janezic and J. A. Jargon, "Complex permittivity determination from propagation constant measurements," *IEEE Microw. Guided Wave Lett.*, vol. 9, no. 2, pp. 76–78, Feb. 1999.

[11] B. A. Sanadiki and M. Mostafavi, "Inversion of inhomogeneous continuously varying dielectric profiles using open-ended waveguides," *IEEE Trans. Antennas Propag.*, vol. 39, no. 2, pp. 158–163, Feb. 1991.

[12] "Agilent 85071E materials measurement software: Technical overview," Agilent Technol., Palo Alto, CA, 2003.

[13] "The measurement of both permittivity and permeability of solid materials"," Hewlett-Packard Company, Palo Alto, CA, Product note on Hewlett-Packard 85071 materials measurement software.

[14] D. Pozar, *Microwave Engineering*, 3rd ed. New York: Wiley, 2003.

[15] R. Ludwig and P. Bretchko, *RF Circuit Design: Theory and Applications*. Upper Saddle River, NJ: Prentice-Hall, 2000.

[16] J. J. More, "The Levenberg–Marquardt algorithm: Implementation and theory," in *Numerical Analysis*, G. A. Watson, Ed. Berlin, Germany: Springer-Verlag, 1977, vol. 630, Lecture Notes Math., pp. 105–116.

[17] M. C. Biggs, "Constrained minimization using recursive quadratic programming," in *Toward Global Optimization*, L. C. W. Dixon and G. P. Szergo, Eds. Amsterdam, The Netherlands, North-Holland, 1975, pp. 341–349.
[18] N. Metropolis, A. Rosenbluth, M. Rosenbluth, A. Teller, and E. Teller, "Equation of state calculations by fast computing machines," *J. Chem. Phys.*, vol. 21, no. 6, pp. 1087–1092, Jun. 1953.
[19] D. E. Goldberg, *Genetic Algorithms in Search, Optimization, and Machine Learning*. New York: Addison-Wesley, 1989.
[20] K. Schittkowski, "NLQPL: A fortran-subroutine solving constrained nonlinear programming problems," *Ann. Oper. Res.*, vol. 5, pp. 485–500, 1985/1986.
[21] R. Fletcher, *Practical Methods of Optimization*, 2nd ed. New York: Wile, 2000.
[22] P. E. Gill, W. Murray, and M. H. Wright, *Practical Optimization*. San Diego, CA: Academic, 1981.
[23] S. P. Han, "A globally convergent method for nonlinear programming," *J. Optim. Theory Appl.*, vol. 22, no. 3, pp. 297–309, Jul. 1977.
[24] W. Hock and K. Schittowski, "A comparative performance evaluation of 27 nonlinear programming codes," *Computing*, vol. 30, no. 4, pp. 335–354, Apr. 1983.
[25] R. L. Haupt, "An introduction to genetic algorithms for electromagnetics," *IEEE Antennas Propag. Mag.*, vol. 37, no. 2, pp. 7–15, Apr. 1995.
[26] J. M. Johnson and Y. Rahmat-Samii, "Genetic algorithms in engineering electromagnetics," *IEEE Antennas Propag. Mag.*, vol. 39, no. 4, pp. 7–21, Aug. 1997.
[27] P. J. Matthews and J. J. Song, *RF Impedance Measurement Calibration* Argonne, IL, 1993, LS Note 223.
[28] *8510C Network Analyzer System Operating and Programming Manual*, Hewlett-Packard, Palo Alto, CA, 1999.

**Michael E. Baginski** (M'87–SM'95) was born in Erie, PA, on October 20, 1957. He received the B.S., M.S., and Ph.D. degrees from Pennsylvania State University, University Park, in 1980, 1984, and 1987, respectively, all in electrical engineering.

He is currently an Associate Professor of Electrical Engineering, Auburn University, Auburn, AL, where he has resided since the completion of his doctorate degree. His research interests include analytic and numerical solutions to transient electromagnetic problems, transient heat flow and solid-state structural analysis using finite-element routines, and the analysis of the RF drying of textile materials, electromagnetic interference (EMI) and electromagnetic compatibility (EMC) characterization of MCMs and printed circuit boards (PCBs), simulation of rapid thermal expansion of metals under the action of large electric currents, $S$-parameter extraction routines, and synthetic aperture radar design and data processing routines. He is listed in *Who's Who in Science and Engineering* and *Who's Who Among America's Teachers*.

Dr. Baginski is a member of Eta Kappa Nu, Sigma Xi, the New York Academy of Sciences, and the IEEE Education and Electromagnetic Compatibility Societies.

**Daniel L. Faircloth** (S'02) received the B.S. and M.S. degrees in electrical engineering from Auburn University, Auburn, AL, in 2002 and 2003, respectively, and is currently working toward the Ph.D. degree in electrical and computer engineering at Auburn University.

His research includes finite-element analysis of transient and steady-state electromagnetic phenomena, optimization techniques applicable to electromagnetic design, inverse problems, synthetic aperture radar antenna design, and numerical modeling of landmine and unexploded ordnance (UXO) problems.

Mr. Faircloth is a member of Eta Kappa Nu, Tau Beta Pi, and Phi Kappa Phi. He was the recipient of a NASA Graduate Student Researchers Program (GSRP) Fellowship.

**Manohar D. Deshpande** (M'02–SM'04) received the B.E. degree in electrical engineering from the Vishveshvarya Regional College of Engineering, Nagpur, India, in 1970, and the M.Tech. and Ph.D. degrees in microwave and radar engineering from the Indian Institute of Technology, Kharagpur, India, in 1972 and 1980, respectively.

In 1975, he joined the faculty of the Indian Institute of Technology. From 1980 to 1982, he was a Post-Doctoral Fellow with George Washington University, Washington, DC, where he developed the integral-equation method to analyze microstrip patch antennas. As a Senior National Research Council (NRC) Resident Research Associate from 1987 to 1989 at the NASA Langley Research Center, Hampton, VA, he was involved with the analysis of finite printed circuit array antennas. Since 1989, he has been a Research Engineer with the NASA Langley Research Center, where he is involved in the development of the hybrid finite-element method and integral-equation approach to analyze electromagnetic scattering and radiation from three-dimensional complex objects.